Eur Radiol (2005) 15: 2497–2505
DOI 10.1007/s00330-005-2873-z

EXPERIMENTAL

Cedric de Bazelaire
Nathalie Siauve
Laure Fournier
Frederique Frouin
Philippe Robert
Olivier Clement
Eric de Kerviler
Charles Andre Cuenod

Comprehensive model for simultaneous MRI determination of perfusion and permeability using a blood-pool agent in rats rhabdomyosarcoma

Received: 20 January 2005
Revised: 21 June 2005
Accepted: 1 July 2005
Published online: 23 August 2005

C. de Bazelaire (✉)
Radiology Department,
Saint Louis Hospital,
1 Avenue Claude Vellefaux,
75475 Paris Cedex 10, France
e-mail: cedric.de-bazelaire@sls.aphp.fr
Tel.: +33-1-42499128
Fax: +33-1-42494468

N. Siauve · L. Fournier · O. Clement ·
E. de Kerviler · C. A. Cuenod
Radiology Department,
George Pompidou European Hospital,
Paris, France

F. Frouin
Faculté de Médecine Pitié-Salpétrière,
INSERM U494,
Paris, France

P. Robert
Recherche et Développement,
Guerbet Laboratoire Guerbet,
Paris, France

Abstract To present a new compartmental analysis model developed to simultaneously measure tissue perfusion and capillary permeability in a tumor using MRI and a macromolecular contrast medium. Rhadomyosarcomas were implanted subcutaneously in 20 rats and studied by 1.5-T MRI using a fast gradient echo sequence (2D fast SPGR TR/TE/α 13 ms/1.2 ms/60°) after injection of a macromolecular contrast medium. The left ventricle and tumor signal intensities were converted into concentrations and modeled using compartmental analysis, yielding tumor perfusion F, distribution volume $V_{distribution}$, volume transfer constant K^{trans}, rate constant of influx k_{pe}, and initial extraction (fraction) E. Tumor perfusion was F=43±29 ml·min^{-1}·100 g^{-1}. The permeability study allowed the measurement of k_{pe}=0.37±0.12 min^{-1} and K^{trans}=0.01±0.0031 min^{-1}. The blood volume could be assimilated to the distribution volume ($V_{distribution}$=2.9±1.01%) since the capillary leakage was small. The simultaneous assessment of perfusion and permeability allowed quantification of the initial extraction (fraction) E=2.34±1.05%. Quantification of both tumor perfusion and capillary leakage is feasible using MRI using a macromolecular blood pool agent. The method should improve tumor characterization.

Keywords Perfusion · Permeability · Mathematical model · Compartmental analysis · Magnetic resonance imaging

Introduction

Use of contrast enhancement in imaging provides a means of evaluating both tissue function and tissue morphology. Contrast enhancement of a lesion can be linked to the development of blood vessels leading to an increase in blood volume and blood flow, defining tissue perfusion. Enhancement can also be related to the extravasations of contrast medium (CM) across the microvascular endothelial barriers toward the interstitial tissue, defining capillary permeability [1]. Kinetic analysis of enhancement may discriminate between perfusion and permeability and improve the specificity of imaging examinations. In benign vascular malformations, there is an increase in perfusion with normal permeability [2]. In aggressive tumors, the increase in permeability and perfusion is necessary for its continued growth. Hyperpermeability and the high number of cancer microvessels in these lesions are mediated by angiogenesis factors, including the vascular endothelial growth factor secreted by the tumor cells [3]. Use of an antiangiogenic compound targeting these factors seems to offer a promising new approach to cancer treatment [4].

However, the monitoring of their therapeutic effect requires new highly sensitive imaging tools, capable of reflecting the changes in the vascular characteristics of tumors. Detection of early decreases in permeability and perfusion, before any morphological modifications, could help evaluating the efficiency of these new antiangiogenic compounds [5].

Three physiological components in tracer distribution can be resolved. The first component is perfusion, which corresponds to the intravascular distribution of the tracer. Perfusion is characterized by the blood flow per unit mass of tissue F ($ml \cdot min^{-1} \cdot 100\ g^{-1}$) and the fractional plasma volume per unit of tissue ν_p (%). The second component is permeability, which describes exchanges across the capillary membrane. Absolute and relative permeability can be characterized by any of the following: the influx rate constant from plasma to interstitial water space k_{pe} (min^{-1}), the efflux rate constant from interstitial space to plasma k_{ep} (min^{-1}) or the influx volume transfer constant K^{trans} (min^{-1}) equal to the product of the transfer constant and the blood volume. Perfusion and permeability are linked, and the initial extraction fraction E (%) is a useful parameter reflecting both components. Diffusion in the interstitial space is a third component of biodistribution. Diffusion could be indirectly characterized by the volume of distribution of a tracer into this space, which is the fractional extravascular extracellular space per unit of tissue ν_e (%).

The abnormally high number and permeability of microvessels in cancers can be assessed quantitatively using MRI enhanced with CM. Three main models have been used for assessment to microcirculation parameters [6]. The Kety [7] model applied to MRI data by both Larson et al. [8] and Tofts and Kermode [9], yielding K^{trans} and ν_e. However, the direct vascular contribution to the tumor signal was ignored in the model leading to an overestimation of the permeability K^{trans}. A second model included a vascular term [10] and has been used to analyze MR data in number of studies [11], and allowed measurement of ν_b in addition to permeability. The third model, recently described by St. Lawrence and Lee [12], potentially enables the estimation of F and K^{trans} separately. However, the estimates obtained using this model varied as a function of the starting values used for the curve fitting and different combinations of parameter produced very similar solutions [6].

This study describes a new model of compartmental analysis using contrast-enhanced MRI in a rat rhabdomyosarcoma model, allowing assessing microcirculation in tumor, along with tissue perfusion and capillary permeability. We also quantified the behavior of a blood pool agent in the tumor.

Materials and methods

Animal and tumoral model

All animal experiments were performed in accordance with the National Institutes of Health recommendations. Ten 12-week-old female AG-Wistar rats (Charles River, Germany), weighting 160–180 g were used. Experiments were performed under anesthesia by means of intraperitoneal injection of a 50/50 mix of xylazine (10 mg/kg, Rompun, Bayer, Leverkusen, Germany) and ketamine (50 mg/kg, Imalgene, Bayer). The tumor model was a rhabdomyosarcoma [13] implanted subcutaneously bilaterally in the flanks of each animal (at the level of the heart) by means of injection of 0.2 ml cell S4MH (provided by M.F. Poupon, Institut Curie, Paris, France) diluted in 1 ml fetal calf serum. For each tumor 2×10^5 cells were injected. Tumors were allowed to grow to approx. 10 mm (range 8–19 mm) in diameter before MRI was performed. Typically rhabdomyosarcomas were imaged 10 days after implantation. For CM injection during MRI a 23-gauge butterfly cannula was inserted into a tail vein of each animal.

Macromolecular contrast medium

P792 (Vistarem, Laboratoire Guerbet, Roissy Charles de Gaulle, France) is a prototypic macromolecular CM [14, 15]. It is a gadolinium chelate with a molecular weight of 6.47 kDa, considered to be a rapid clearance blood pool agent. The relaxation of Vistarem was 29 $l \cdot mmol^{-1} \cdot s^{-1}$ at 37°C and 1.5 T, which is ten times superior to the relaxation of the gadoterate meglumine (Gd-DOTA, Dotarem, Laboratoire Guerbet), a conventional extracellular paramagnetic contrast agent. Vistarem was used for tissue perfusion and capillary permeability measurements at a dose of 0.015 mmol/kg.

Magnetic resonance imaging

MRI was performed with a 1.5-T scanner (Signa Horizon LX2, General Electric, Buc, France) using the body coil for transmit and a knee coil for reception. Animals were placed supine in the knee coil (30 cm long, 20 cm inner diameter). Phantoms containing dilutions of macromolecular CM were included in the field of view next to each animal. Sixteen phantoms with increasing concentrations from 0 to 6 mmol Gd/l Vistarem were used. Unmineralized water was used for dilution. A fast spin-echo sequence in the axial plane was performed to find the best slice level including the left ventricle and both tumors.

For the dynamic postcontrast study tumors were examined using a T1-weighted, high temporal resolution, two-dimensional gradient-refocused acquisition in a steady-

state spoiled gradient recalled sequence. Images were obtained with the following parameters: TR 13 ms, TE 1.2 ms, 25° flip angle, 256×128 matrix, 5 mm section thickness, 14×3.5 cm field of view (phase field of view 0.25), voxel size 0.5×1×5 mm, Nex=1, and acquisition time 0.6 s per slice. Ten initial pre-CM images and 300 dynamic post-CM images were acquired over 3 min to monitor contrast enhancement. Inflow artifacts were reduced using a presaturation slab (thickness of 25 mm and a 10-mm gap between saturation slab and imaged slice). Saturation parameters were defined empirically and care was exercised in selecting thickness and gap to avoid imaged slice saturation.

Data analysis

All raw amplitude images were saved and transferred to a workstation for processing. Signal intensity values for each time point were measured in regions of interest defined in the tumors, the left ventricle, and the gadolinium phantoms. The signal intensity values of phantoms were used to correct for spectrometer variations over time and to convert signal intensity values of the left ventricle and tumors into concentrations for the compartmental analysis. The T1 value of each phantom at 0.47 T and 37°C was measured with a spectrometer (Minispec NMS 120, Bruker). They were converted by means of specific relaxivity r1 of the macromolecular CM to obtain their T1 at 1.5 T [16]. Using the signal intensity measured on MRI during the dynamic acquisition and the calculated T1 value for each phantom of macromolecular CM, curves linking T1 and signal intensity were fitted using the inverted signal intensity equation of two-dimensional fast spoiled gradient recalled acquisition sequences:

The steady-state Bloch equation for a two-dimensional fast spoiled gradient recalled sequence [17] is:

$$IS = m0.\sin\alpha\cdot\exp\left(-\frac{TE}{T2*}\right).\frac{1-\exp\left(-\frac{TR}{T1}\right)}{1-\cos\alpha\cdot\exp\left(-\frac{TR}{T1}\right)} \quad (1)$$

That for the inverted steady-state Bloch equation is:

$$\frac{1}{T1} = \frac{1}{TR}\cdot\ln\frac{1-\cos\alpha\cdot IS}{1-IS} \quad (2)$$

where T1 is the longitudinal relaxation time measured with the spectrometer, TR the repetition time, α the flip angle, and IS the MRI signal intensity. The term m0 is a calibration constant that includes the proton density, the sensitivity of the coils, and the gain of the MR imager. Inversion of Eq. (1) allows elimination of m0. This equation should also include an exp(−TE/T2*) term. It was assumed equal to one because the TE was very small compared to T2*. These fitted curves were used to obtain the relaxation rate values (1/T1) from the signal intensity values of the left ventricle and tumors during the dynamic acquisition in MRI. Pre- and post-CM relaxation rates (1/T1) were obtained with the same technique. Changes in the relaxation rate between the pre- and post-CM region of interest at any time [Δ1/T1(t)] were calculated according to:

$$\Delta 1/T1(t) = \frac{1}{T1_{post}(t)} - \frac{1}{T1_{pre}} \quad (3)$$

where $T1_{pre}$ is the value of T1 before injection of any tracer. We assumed Δ1/T1(t) to be directly proportional to the gadolinium concentration C(t):

$$\Delta 1/T1(t) = r1\cdot C(t) \quad (4)$$

where C(t) is the tracer concentration in voxel ($mmol\cdot l^{-1}$) and r1 the relaxivity ($l\cdot mmol^{-1}\cdot s^{-1}$). Δ1/T1(t) is also proportional to the CM amount ($q_{voxel;}$ mmol), per voxel volume (V_{voxel}; l):

$$\Delta 1/T1(t) = r1\cdot\frac{q_{voxel}(t)}{V_{voxel}} \quad (5)$$

Kinetic analysis of Δ1/T1(t) data from the tumor and left ventricle was performed with a compartmental and numerical modeling program (SAAM II, SAAM Institute, Seattle, Wash., USA). According to the CM biodistribution in the capillary and interstitial space, an open bicompartmental pharmacokinetic model was created with capillary and interstitial compartments (Fig. 1). We assumed that the exchanges from capillary to interstitial space symbolized by the influx rate constant $k_{3,2}$ (min^{-1})

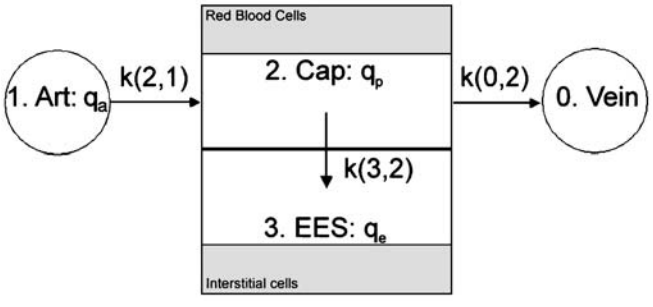

Fig. 1 The perfusion-permeability model. An open two-compartment model was used to describe the transport of CM through the capillaries and its monodirectional diffusion between the plasma (q_p mean amount) and the interstitial space (q_e mean amount) symbolized by the influx rate constant $k_{3,2}$ through the capillary wall; q_a CM amount in the feeding artery; $k_{2,1}$ rate constant of influx from artery to capillary; $k_{0,2}$ rate constant of efflux from the capillary to the venous system

are governed by diffusion following the concentration gradient. We assumed that the reflux of the blood pool agent from the interstitial space back to the capillary is negligible at the early phase (first pass and preequilibrium) when CM interstitial concentration is near zero [18]. The capillary compartment receives the arterial influx rate constant $k_{2,1}$ (min^{-1}). The constant $k_{0,2}$ symbolizes the venous efflux rate constant. In this model the differential equation describing the variations in the amount of CM over time in the capillary and interstitial compartments followed two equations such as the following. For the capillary compartment this was:

$$\frac{d(q_p(t))}{dt} = k_{2,1} \cdot q_a(t) - k_{3,2} \cdot q_p(t) - k_{0,2} \cdot q_p(t) \quad (6)$$

where q_p and q_a (mmol) are, respectively, the plasmatic amounts of CM within the capillary and the arterial compartments, $k_{2,1} \times q_a$ ($mmol \cdot min^{-1}$) the arterial input amount of CM in the capillary compartment, $k_{3,2} \times q_p$ ($mmol \cdot min^{-1}$) the CM amount that passed from the capillary to the interstitial space, and $k_{0,2} \times q_p$ ($mmol \cdot min^{-1}$) the venous output amount of CM. For the interstitial space it was:

$$\frac{d(q_e(t))}{dt} = k_{3,2} \cdot q_p(t) \quad (7)$$

where q_e (mmol) is the CM amount in the interstitial compartment, and $k_{3,2} \times q_p$ ($mmol \cdot min^{-1}$) the influx CM amount in interstitial space.

SAAM II solved the model and fitted it to the observed values of $\Delta 1/T1$ obtained from MRI in the tumors and left ventricle (including the first 150 s), yielding $k_{2,1}$, $k_{3,2}$, $k_{0,2}$ and the variation over time of the amount of tracer within the interstitial and capillary compartments. The blood flow (F), the fractional plasma volume (ν_p), the volume transfer constant (K^{trans}), the influx rate constant (k_{pe}), and the extraction fraction (E) were deduced from $k_{2,1}$, $k_{3,2}$, and $k_{0,2}$ using Fick's general equation of mass balance which, applied to the open two-compartmental model, describes the transport of a contrast medium through the plasma compartment and its leakage into the interstitial space [19]:

$$\begin{aligned}\frac{d(q_p(t))}{dt} &= F \cdot M_{voxel} \cdot (C_a(t) - C_v(t)) \\ &\quad - P \cdot S \cdot M_{voxel} \cdot (C_p(t) - C_e(t))\end{aligned} \quad (8)$$

where F is the flow of plasma per unit mass ($ml \cdot min^{-1} \cdot 100\ g^{-1}$), M_{voxel} the mass of the tissue in the voxel (g), P the permeability constant per unit concentration difference and per unit area of semipermeable membrane, S the area of the membrane per unit mass of tissue (PS product; $ml \cdot min^{-1} \cdot 100\ g^{-1}$). C_a, C_v, C_p, and C_e are the concentrations of CM in arterial plasma, venous plasma, capillary plasma, and the extravascular extracellular space, respectively ($mmol\ l^{-1}$). The product $F \times M_{voxel} \times (C_a - C_v)$ is the arterial amount of CM received by the capillary compartment ($mmol \cdot min^{-1}$), $P \times S \times M_{voxel} \times (C_p - C_e)$ represents the exchanges of CM between the capillary and interstitial space ($mmol \cdot min^{-1}$). All parameters were obtained by analogy between Eqs. (6) and (8) using the flow and the permeability components as described in the Appendix.

Comparison with literature values

Statistical analysis was performed using Stat-View 5.0 (SAS Institute, Cary, N.C., USA) on a workstation. Our volume transfer constants and fractional blood volumes were compared to values found in the literature with Vistarem as CM in experimental breast cancer with comparable histological tumor grade implanted in Sprague–Dawley rats [20]. In this study Turetschek et al. [20] employed a two-compartment bidirectional model to assess K^{trans} and ν_p. There was no study measuring blood flow in tumor with Vistarem available in the literature. For this reason our values of F were compared to values obtained in experimental breast cancer implanted on Fisher rats with fluorescent microspheres publish by Daldrup et al. [21]. Our values of perfusion and permeability were compared with literature values using the nonparametric Mann–Whitney test. For each rats mean values of K^{trans}, F, and ν_p of the couple of tumors were calculated to respect the assumptions of independence between samples.

Results

Of the 20 rhabdomyosarcomas in ten rats, 19 were successfully studied with this early phase model; one exhibited insufficient growth (less than 5 mm) and was excluded from the study. Macroscopic examination showed well-encapsulated, vascular soft tumors with a small central area of necrosis.

The macromolecular CM was well tolerated by the rats. After injection of CM the enhancement in the left ventricle was noticeably higher than in the subcutaneous rhabdomyosarcomas as shown in (Fig. 2c,d). The signal-to-noise ratio (SNR) was found to be 6.0 in heart and 15.7 in tumor before injection. The SNR in left ventricle and tumor, calculated between 100 and 160 s (when enhancement plateaus) were found to be 9.5 and 32.0, respectively. The low achieved SNR here was probably due to a relatively small dose of administered contrast agent and the small distribution volume of the macromolecule in the tumor tissue. The curves of SI measured over time obtained from the dynamic MRI data in the left ventricle after intravenous bolus administration of macromolecular CM were con-

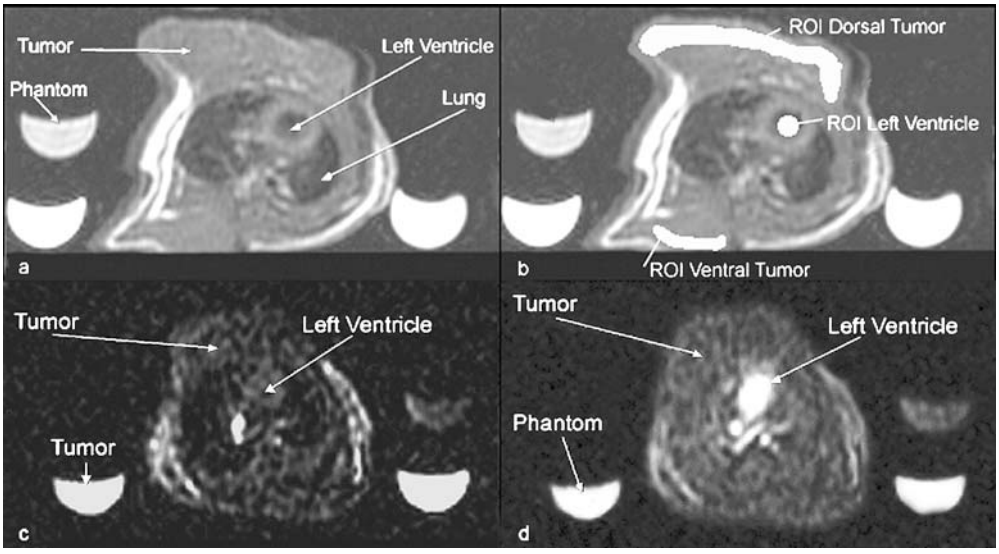

Fig. 2 Axial MRI images of tumors at the level of the heart. *Clusters 2a, 2b* MRI images at 1.5-T obtained with the fast spin echo sequence for localization. ROI (*white areas*) were placed on a transverse slice through the heart, dorsal and ventral tumors. *Clusters 2c* (precontrast) and *2d* (15 s postcontrast) present in a different animal representative axial T1-weighted SPGR images of a subcutaneous rhabdomyosarcoma using the macromolecular CM. Note the very strong enhancement in the left ventricle relative to the tumor

verted into Δ1/T1 kinetics, which were proportional to concentrations curves (Fig. 3). The kinetics of the Δ1/T1 value in the left ventricle presented a pre-CM phase, the first pass lasting 5 s, a second pass, and a preequilibrium phase. Figure 4a presents a representative least squares fit of the model with Δ1/T1 measures of dynamic MRI data obtained in the tumor. In tumor the Δ1/T1 values increased substantially until 60–80 s after injection, with a fast increase during the first pass followed by a slower increase. Figure 4b shows typical capillary and interstitial space adjusted responses using the SAAM II software of the early phase model with macromolecular CM. As predicted by the assumption of monodirectional exchanges, all Δ1/T1

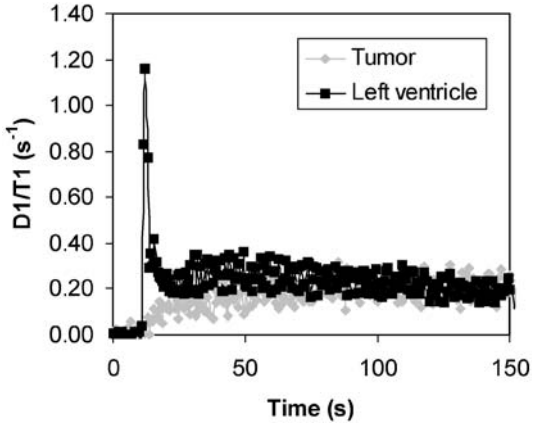

Fig. 3 Example of Δ1/T1 kinetics in blood and tumor as a function of time. Δ1/T1 values were obtained from signal intensities measured with ROI defined in heart and tumor as shown Fig. 2b. Signal intensities were converted into Δ1/T1 using a calibration curve established with phantoms of dilution of CM. Arterial curves showed a first pass followed by a second pass. Rhadomyosarcoma shows a slowly increasing enhancement over time, whereas the enhancement of blood vessels in the field of view decreased

values of the interstitial compartment increased continuously. The Δ1/T1 value of the capillary space showed a rapidly increasing component corresponding to the first pass and a less rapidy increasing component during the second pass, followed by a declining component. This last declining part of Δ1/T1 of the capillary space, whereas Δ1/T1 in the interstitium continuously increased, was indicative of a substantial microvascular leakage with progressive accumulation of CM in the interstitial space of the tumor. It appeared from this curves that the equilibrium phase should be reached after 140 s following injection.

Table 1 shows values obtained with the model for the influx rate constant from plasma to interstitial space (k_{pe}=0.37±0.12 min^{-1}), influx volume transfer constant into interstitial space (K^{trans}=0.01±0.0031 min^{-1}), blood flow (F=43 ±29.4 $ml \cdot min^{-1} \cdot 100\ g^{-1}$), fractional plasma volume (ν_p=2.94±1.01%), and extraction ratio of macromolecular CM in tumor (E=2.34±1.05%).

The accuracy of the technique was evaluated by comparison with results found in the literature [20, 22] for K^{trans}, F, and ν_p. Higher perfusion values in rhabdomyosarcomas were found in our study than those published by Daldrup et al. [21, 22] in experimental breast cancer investigated using fluorescent microspheres (F=24 $ml \cdot min^{-1} \cdot 100\ g^{-1}$, P=0.01). Our permeability and fractional plasma volume assessments were compared to results found in experimental breast cancer with Vistarem by Turetschek et al. [20]. Similar permeability values (K^{trans}=0.006 min^{-1}, P>0.05) were found between rhabdomyosarcoma and breast cancer with high Scarff–Bloom–Richardson score (SBR >6). However, permeability values were significantly lower (K^{trans}=0.004 min^{-1}, P<0.001) in breast cancer with lower score (SBR<5). No difference in fractional plasma volume was found between our results and those reported by Turetschek et al. (ν_p=0.04, P>0.2).

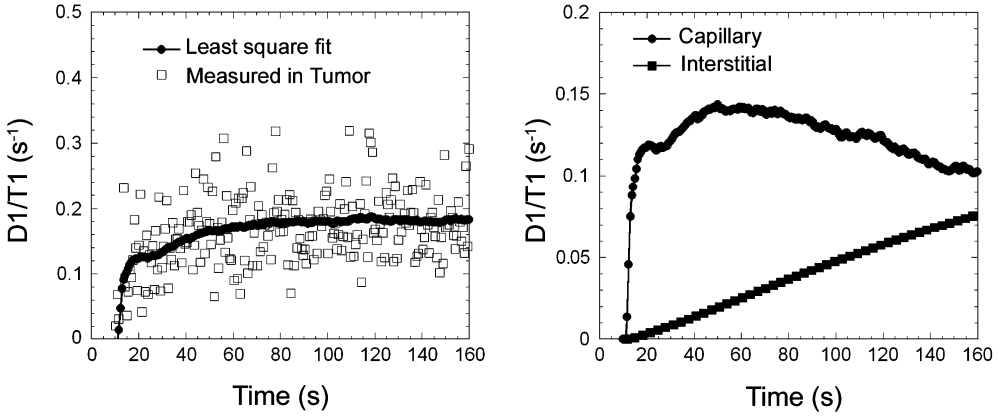

Fig. 4 Typical tumor Δ1/T1 curve over time. **a** Typical Δ1/T1 measures over time obtained in the tumor after intravenous bolus administration of macromolecular CM in rats, as well as the least square fit of the dynamic MRI data using our early-phase model. The Δ1/T1 value in the tumor increased rapidly during the first pass followed by a slower increase and the steady state. The equilibrium phase was reached after 140 s postinjection. **b** Capillary (*circle*) and interstitial (*square*) curves generated by the application of the compartmental model to the total tumor enhancement. It is indicative of a substantial microvascular leakage with progressive accumulation of CM in the interstitial space of the tumor. Transport through the capillary wall was governed by the CM gradient between plasma and interstitial space, which gradient decreases during the course of the experience. For this reason the interstitial curve showed a slight inflexion after 130 s

Discussion

The present study defines a new pharmacokinetic model, that simultaneously considers capillary blood supply and leakage of macromolecular contrast medium from the plasma to the interstitial tissue compartment. Our method combines fit of completion into the capillary and the extravascular space, and perfusion and permeability measurements.

Table 1 Perfusion and permeability parameters obtained with the early phase model using the macromolecular contrast media

Rat no.	Tumor no.	F (ml min^{-1} per 100 g)	k_{pe} (min^{-1})	K^{trans} (min^{-1})	ν_p (%)	E (%)
1	1	23.5	0.22	0.0069	3.14	2.95
	2	46.0	0.34	0.0093	2.73	2.02
2	3	103.8	0.39	0.0175	4.50	1.69
	4	125.0	0.21	0.0114	5.42	0.91
3	5	73.0	0.60	0.0140	2.33	1.92
	6	45.9	0.29	0.0123	4.23	2.67
4	7	30.0	0.18	0.0058	3.24	1.94
5	8	32.7	0.37	0.0128	3.47	3.92
	9	20.0	0.43	0.0091	2.11	4.53
6	10	47.5	0.47	0.0092	1.96	1.94
	11	18.3	0.35	0.0102	2.92	5.59
7	12	24.0	0.25	0.0060	2.39	2.49
	13	19.9	0.42	0.0099	2.36	4.98
8	14	33.7	0.40	0.0066	1.64	1.94
	15	32.3	0.23	0.0086	3.76	2.67
9	16	46.0	0.51	0.0120	2.36	2.62
10	17	36.6	0.47	0.0083	1.76	2.26
	18	22.1	0.48	0.0128	2.67	5.81
Mean ±SD		43.3±29.4	0.37 ±0.12	0.0102 ±0.0031	2.94 ±1.01	2.34 ±1.05

The present study defines a new pharmacokinetic model, that simultaneously considers capillary blood supply and leakage of macromolecular contrast medium from the plasma to the interstitial tissue compartment. Our method combines fit of completion into the capillary and the extravascular space, and perfusion and permeability measurements.

We quantified blood flow (F=43 ml·min^{-1}·100 g^{-1}), and fractional plasma volume (ν_p=3%). Perfusion was quantifiable using a macromolecular CM with a slow leakage into the extravascular space. In pharmacokinetic analysis, when a macromolecular CM is used, the initial rising phase in the measured tumor enhancement time course after CM injection is attributed to the vascular fraction of the tissue. In addition, tracer concentration changes in the vascular compartment depend more on flow than permeability with a macromolecular CM. Thus we were able to obtain blood flow from the completion of capillary space. With a small molecular CM interstitial permeability is not negligible in the early phase, and the separation of the plasmatic and interstitial phases is more difficult. Fractional plasma volume was quantified using the biodistribution of the macromolecular CM. With the low rate of extravasation of the macromolecular CM the dilution volume of CM can be equivalent to the plasma volume, at least at an early phase postinjection. The permeability was estimated using the influx volume transfer constant into the interstitial space (K^{trans}=0.01 min^{-1}) and the influx rate constant from plasma to interstitial space (k_{pe}=0.37 min^{-1}). Permeability was measurable after the first pass, when the intravascular component was no longer dominant. The extraction fraction, reflecting both perfusion and permeability, could be quantified with the early phase model. We found a low extraction fraction (E=2%) in the subcutaneous rhabdomyosarcoma with the macromolecular CM.

In the literature reports of simultaneous analysis of perfusion and permeability using MRI are rare. While permeability is usually accurately characterized (e.g., with

K^{trans}), few additional parameters are measured. Perfusion measurements in extracerebral tissues are not common. Brix et al. [19] published a two-compartmental model for assessing perfusion and permeability using computed tomography, yielding perfusion and permeability parameters. Unfortunately, such a study is limited in clinical practice by its high radiation exposure for patients.

The SAAM II software for compartmental analysis was used to compute our imaging data. The following assumptions were made to simplify our equations: (a) the volume of the voxel in the left ventricle contained only blood, and therefore $V_{plasma}/V_{voxel}=V_{plasma}/V_{blood}$=1-hematocrit. (b) Because we used a macromolecular CM with low leakage, it could be assumed that exchanges were monodirectional between compartments. We neglected the reflux of this blood pool agent from the interstitial space back to plasma at the initial phase postinjection, when the CM capillary concentration was much higher than the CM interstitial concentration. This assumption was in agreement with results published by Daldrup–Link and Brasch [23]. Tardivon et al. [18] found that invasive carcinomas do not show a washout pattern up to 35 min after P792 injection but rather a slowly increasing enhancement over time, whereas the enhancement of blood vessels in the field of view decreased.

Bolus injections of macromolecular CM have not yet been approved in humans. However, macromolecular CM was essential for the implementation of the early phase model. The slow pharmacokinetics of macromolecular CM allowed adequate sampling of the first pass in MRI, which was not possible with small molecular CM. The first results in clinical studies in patients using Vistarem show excellent tolerance, which is encouraging for the future application of our models in humans.

There is no suitable validation method in functional imaging. The blood flows measured in the rhadomyosarcoma implanted in our rats were higher than perfusion values found by Daldrup with microspheres in experimental breast cancer developed in rat. This difference may be due to specific histological differences between the two cancers. Our perfusion values may be overestimated by the assumption of tissue density value (ρ=1) [24, 25]. Similar K^{trans} were found in our tumors and in experimental breast cancers with high SBR score implanted in rats [20]. However, in this study Turetschek et al. found also permeability values for breast cancer model with lower malignancy grade (SBR score), which differed significantly from our results. These findings are in good agreement with the hypothesis of an increase in capillary permeability in cancer [23]. No significant difference was found between our fractional plasma volumes and values reported by Turetschek et al. (for all SBR scores). This finding may indicate that fractional plasma volume is a less sensitive surrogate of malignancy than K^{trans}.

Conclusion

The proposed kinetic analysis of dynamic MRI data allows simultaneous quantification of perfusion and permeability. This approach offers promising prospects for quantitative characterization of tissue microcirculation. In our laboratory we used this technique to investigate anti-vascular endothelial growth factor treatment (Astra-Zeneca Pharmaceuticals, Alderly Park, UK). We observed a significant decrease in blood flow, blood volume, and permeability 24 h after administration of treatment [26]. In the future our model may be applied to monitor changes in tumor microvascular characteristics after treatment in patients, after validation in animal models, improving the standard morphological imaging by adding a functional dimension.

Acknowledgements We wish to acknowledge Dr. Marie France Poupon (Institut Curie, Paris, France) for providing us with the S4MH cell lines. Work supported in part by the William D. Coolidge grant of the European Congress of Radiology (C.A.C.).

Appendix

The blood flow (F), the fractional plasma volume (ν_p), the volume transfer constant (K^{trans}), the influx rate constant (k_{pe}), and the extraction fraction (E) were deduced from $k_{2,1}$, $k_{3,2}$, and $k_{0,2}$, using Fick's general equation of mass balance, which applied to the open two-compartmental model describes the transport of a contrast medium through the plasma compartment and its leakage into the interstitial space [19]:

Equation (8) can also be written as:

$$\frac{1}{V_{voxel}}\cdot\frac{d\left(q_p(t)\right)}{dt}=F\cdot\frac{M_{voxel}}{V_{voxel}}\cdot\left(C_a(t)-C_V(t)\right)-P\cdot S\cdot\frac{M_{voxel}}{V_{voxel}}\cdot\left(C_p(t)-C_e(t)\right) \tag{9}$$

where V_{voxel} is the volume of a voxel. Using the tissue density of the voxel (ρ=M/V) Eq. (9) becomes:

$$\frac{1}{V_{voxel}}\cdot\frac{d\left(q_p(t)\right)}{dt}=F\cdot\rho\cdot\left(C_a(t)-C_V(t)\right)-P\cdot S\cdot\rho\cdot\left(C_p(t)-C_e(t)\right) \tag{10}$$

By analogy with Eq. (6) of the model, Eq. (10) can be written:

$$\frac{1}{V_{voxel}}\cdot\frac{d\left(q_p(t)\right)}{dt}=F\cdot\rho\cdot C_a(t)-P\cdot S\cdot\rho\cdot\left(C_p(t)-C_e(t)\right)-F\cdot\rho\cdot C_v(t) \tag{11}$$

$C_v(t)$, the concentration in venous plasma at the exit of the capillary, is assumed to be equal to the concentration in capillary plasma $C_p(t)$ giving:

$$\frac{1}{V_{voxel}} \cdot \frac{d\left(q_p(t)\right)}{dt} = F \cdot \rho \cdot C_a(t) - P \cdot S \cdot \rho \cdot \left(C_p(t) - C_e(t)\right) - F \cdot \rho \cdot C_p(t) \quad (12)$$

All parameters were obtained by analogy between Eq. (6) (derived from our compartmental model used with SAAM II) and Eq. (12) (derived from general equation of mass balance) separating the flow and the permeability components:

For flow, the analogy of the amount of CM received by the capillary compartment yields:

$$V_{voxel} \cdot F \cdot \rho \cdot C_a(t) \Leftrightarrow k_{2,1} \cdot q_a(t) \quad (13)$$

In other words, in Eq. (13), the left side (derived from the general equation of mass balance) is considered equivalent to the right side (derived from our imaging compartmental model).

In MRI the extracellular CM concentration is measured in the whole blood volume (Cb). Therefore a correction of C_b by the hematocrit (Ht approx. 0.45) is necessary:

$$q_a(t) = V_{voxel} \cdot C_a(t) = V_{voxel} \cdot \frac{C_b(t)}{1 - Ht} \quad (14)$$

Using Eq. (14), Eq. (13) becomes:

$$F \cdot \rho \cdot C_a(t) \Leftrightarrow k_{2,1} \cdot C_a(t) = k_{2,1} \cdot \frac{C_b(t)}{1 - Ht} \quad (15)$$

The product $F \times \rho \times C_a(t)$ is equivalent to the product $k_{2,1} \times C_b(t)/(1\text{-}Ht)$. Therefore estimation of $k_{2,1}$ from experimental data $[C_b(t)]$ allows deduction of volume blood flow:

$$F \cdot \rho \Leftrightarrow \frac{k_{2,1}}{1 - Ht} \quad (16)$$

The tissue density (ρ) is assumed to be equal to 1 according to literature values [24, 25].

For permeability, the analogy of exchanges between compartments yields:

$$V_{voxel} \cdot P \cdot S \cdot \rho \cdot \left(C_p(t) - C_e(t)\right) \Leftrightarrow k_{3,2} \cdot q_p(t) \quad (17)$$

Replacing q_p by $\nu_p \times C_p(t) \times V_{voxel}$, Eq. (17) can be simplified into:

$$P \cdot S \cdot \rho \cdot \left(C_p(t) - C_e(t)\right) \Leftrightarrow k_{3,2} \cdot \nu_p \cdot C_p(t) \quad (18)$$

When using a macromolecular CM with a low leakage rate, we can assume that the concentration in the extravascular extracellular space is negligible in comparison with the concentration in the capillary at the beginning of the experiment. The rate constant kpe is deduced from:

$$\frac{P \cdot S \cdot \rho}{\nu_p} \Leftrightarrow k_{3,2}(t) \quad (19)$$

$P \times S \times \rho$ is equal to K^{trans}, and the ratio K^{trans}/ν_p is equal to $k_{pe}(t)$.

For blood volume, the analogy of the venous output yields:

$$V_{voxel} \cdot F \cdot \rho \cdot C_p(t) \Leftrightarrow k_{0,2} \cdot q_p(t) \quad (20)$$

Replacing $q_p(t)$ by $\nu_p \times C_p(t) \times V_{voxel}$ Eq. (20) can be simplified into:

$$F \cdot \rho \cdot C_p(t) \Leftrightarrow k_{0,2} \cdot \nu_p \cdot C_p(t) \quad (21)$$

The plasma volume ν_p is deduced as follows:

$$\nu_p \Leftrightarrow \frac{F \cdot \rho}{k_{0,2}} \quad (22)$$

The extraction fraction E is calculated according to the model of Renkin [27] and Crone [28] of capillary permeability such as:

$$E = 1 - \exp\left(-\frac{K^{trans}}{F}\right) \quad (23)$$

References

1. Jain RK (1987) Transport of molecules across tumor vasculature. Cancer Metastasis Rev 6:559–593
2. Brasch R, Turetschek K (2000) MRI characterization of tumors and grading angiogenesis using macromolecular contrast media: status report. Eur J Radiol 34:148–155
3. Folkman J (1992) The role of angiogenesis in tumor growth. Semin Cancer Biol 3:65–71

4. Folkman J (1971) Tumor angiogenesis: therapeutic implications. N Engl J Med 285:1182–1186
5. Hunter GJ, Hamberg LM, Choi N, Jain RK, McCloud T, Fischman AJ (1998) Dynamic T1-weighted magnetic resonance imaging and positron emission tomography in patients with lung cancer: correlating vascular physiology with glucose metabolism. Clin Cancer Res 4:949–955
6. Buckley DL (2002) Uncertainty in the analysis of tracer kinetics using dynamic contrast-enhanced T1-weighted MRI. Magn Reson Med 47:601–606
7. Kety SS (1951) The theory and applications of the exchange of inert gas at the lungs and tissues. Pharmacol Rev 3:1–41
8. Larsson HB, Stubgaard M, Frederiksen JL, Jensen M, Henriksen O, Paulson OB (1990) Quantitation of blood-brain barrier defect by magnetic resonance imaging and gadolinium-DTPA in patients with multiple sclerosis and brain tumors. Magn Reson Med 16:117–131
9. Tofts PS, Kermode AG (1991) Measurement of the blood-brain barrier permeability and leakage space using dynamic MR imaging. 1. Fundamental concepts. Magn Reson Med 17:357–367
10. Tofts PS (1997) Modeling tracer kinetics in dynamic Gd-DTPA MR imaging. J Magn Reson Imaging 7:91–101
11. Fritz-Hansen T, Rostrup E, Sondergaard L, Ring PB, Amtorp O, Larsson HB (1998) Capillary transfer constant of Gd-DTPA in the myocardium at rest and during vasodilation assessed by MRI. Magn Reson Med 40:922–929
12. St. Lawrence KS, Lee TY (1998) An adiabatic approximation to the tissue homogeneity model for water exchange in the brain. I. Theoretical derivation. J Cereb Blood Flow Metab 18: 1365–1377
13. Antoine E, Pauwels C, Verrelle P, Lascaux V, Poupon MF (1988) In vivo emergence of a highly metastatic tumour cell line from a rat rhabdomyosarcoma after treatment with an alkylating agent. Br J Cancer 57:469–474
14. Port M, Corot C, Raynal I, Idee JM, Dencausse A, Lancelot E, Meyer E, Bonnemain B, Lautrou J (2001) Physicochemical and biological evaluation of P792, a rapid-clearance blood-pool agent for magnetic resonance imaging. Invest Radiol 36:445–454
15. Port M, Corot C, Rousseaux O, Raynal I, Devoldere L, Idee JM, Dencausse A, Le Greneur S, Simonot C, Meyer D (2001) P792: a rapid clearance blood pool agent for magnetic resonance imaging: preliminary results. MAGMA 12:121–127
16. Bottomley PA, Foster TH, Argersinger RE, Pfeifer LM (1984) A review of normal tissue hydrogen NMR relaxation times and relaxation mechanisms from 1–100 MHz: dependence on tissue type, NMR frequency, temperature, species, excision, and age. Med Phys 11:425–448
17. Hittmair K, Gomiscek G, Langenberger K, Recht M, Imhof H, Kramer J (1994) Method for the quantitative assessment of contrast agent uptake in dynamic contrast-enhanced MRI. Magn Reson Med 31:567–571
18. Tardivon A, Guinebretiere JM, Dromain C, Caillet H (2002) MR imaging of breast cancer with a new macocyclic blood pool agent (P792). Eur Radiol 12 (Suppl 1):158
19. Brix G, Bahner ML, Hoffmann U, Horvath A, Schreiber W (1999) Regional blood flow, capillary permeability, and compartmental volumes: measurement with dynamic CT-initial experience. Radiology 210:269–276
20. Turetschek K, Floyd E, Shames DM, Roberts TP, Preda A, Novikov V, Corot C, Carter WO, Brasch RC (2001) Assessment of a rapid clearance blood pool MR contrast medium (P792) for assays of microvascular characteristics in experimental breast tumors with correlations to histopathology. Magn Reson Med 45:880–886
21. Daldrup HE, Shames DM, Husseini W, Wendland MF, Okuhata Y, Brasch RC (1998) Quantification of the extraction fraction for gadopentetate across breast cancer capillaries. Magn Reson Med 40:537–543
22. Daldrup H, Shames DM, Wendland M, Okuhata Y, Link TM, Rosenau W, Lu Y, Brasch RC (1998) Correlation of dynamic contrast-enhanced magnetic resonance imaging with histologic tumor grade: comparison of macromolecular and small-molecular contrast media. Pediatr Radiol 28:67–78
23. Daldrup-Link HE, Brasch RC (2003) Macromolecular contrast agents for MR mammography: current status. Eur Radiol 13:354–365
24. Torlakovic G, Grover VK, Torlakovic E (2005) Easy method of assessing volume of prostate adenocarcinoma from estimated tumor area: using prostate tissue density to bridge gap between percentage involvement and tumor volume. Croat Med J 46:423–428
25. DiResta GR, Lee JB, Arbit E (1991) Measurement of brain tissue specific gravity using pycnometry. J Neurosci Methods 39:245–251
26. Pradel C, Siauve N, Bruneteau G, Clement O, de Bazelaire C, Frouin F, Wedge SR, Tessier JL, Robert PH, Frija G, Cuenod CA (2003) Reduced capillary perfusion and permeability in human tumour xenografts treated with the VEGF signalling inhibitor ZD4190: an in vivo assessment using dynamic MR imaging and macromolecular contrast media. Magn Reson Imaging 21:845–851
27. Renkin E (1959) Transport of potassium-42 from blood to tissue in isolated mammalian skeletal muscles. Am J Physiol 197:1205–1210
28. Crone C (1963) The permeability of capillaries in various organs determined by the use of the “indicator diffusion” method. Acta Physiol Scand 58: 292–305